© 2019. Published by The Company of Biologists Ltd | Journal of Experimental Biology (2019) 222, jeb204172. doi:10.1242/jeb.204172

RESEARCH ARTICLE

Scaling of swimming performance in baleen whales

William T. Gough[1,*], Paolo S. Segre[1], K. C. Bierlich[2], David E. Cade[1], Jean Potvin[3], Frank E. Fish[4], Julian Dale[2], Jacopo di Clemente[5], Ari S. Friedlaender[6], David W. Johnston[2], Shirel R. Kahane-Rapport[1], John Kennedy[3], John H. Long[7], Machiel Oudejans[8], Gwenith Penry[9], Matthew S. Savoca[1], Malene Simon[10], Simone K. A. Videsen[11], Fleur Visser[8,12,13], David N. Wiley[14] and Jeremy A. Goldbogen[1]

ABSTRACT

The scale dependence of locomotor factors has long been studied in comparative biomechanics, but remains poorly understood for animals at the upper extremes of body size. Rorqual baleen whales include the largest animals, but we lack basic kinematic data about their movements and behavior below the ocean surface. Here, we combined morphometrics from aerial drone photogrammetry, whale-borne inertial sensing tag data and hydrodynamic modeling to study the locomotion of five rorqual species. We quantified changes in tail oscillatory frequency and cruising speed for individual whales spanning a threefold variation in body length, corresponding to an order of magnitude variation in estimated body mass. Our results showed that oscillatory frequency decreases with body length ($\propto$length$^{-0.53}$) while cruising speed remains roughly invariant ($\propto$length$^{0.08}$) at 2 m s^{-1}. We compared these measured results for oscillatory frequency against simplified models of an oscillating cantilever beam ($\propto$length^{-1}) and an optimized oscillating Strouhal vortex generator ($\propto$length^{-1}). The difference between our length-scaling exponent and the simplified models suggests that animals are often swimming non-optimally in order to feed or perform other routine behaviors. Cruising speed aligned more closely with an estimate of the optimal speed required to minimize the energetic cost of swimming ($\propto$length$^{0.07}$). Our results are among the first to elucidate the relationships between both oscillatory frequency and cruising speed and body size for free-swimming animals at the largest scale.

KEY WORDS: Morphometrics, Hydrodynamic modeling, Unoccupied aerial systems, Locomotion, Frequency, Speed

[1]Hopkins Marine Station, Stanford University, Pacific Grove, CA 93950, USA. [2]Nicholas School of the Environment, Duke University, Beaufort, NC 28516, USA. [3]Department of Physics, Saint Louis University, St Louis, MO 633103, USA. [4]Department of Biology, West Chester University, West Chester, PA 19383, USA. [5]Accademia del Leviatano, Viale dell'Astronomia, 00144 Rome, Italy. [6]Institute of Marine Sciences, University of California Santa Cruz, Santa Cruz, CA 95064, USA. [7]Departments of Biology and Cognitive Science, Vassar College, Poughkeepsie, NY 12604, USA. [8]Kelp Marine Research, 1624 CJ Hoorn, The Netherlands. [9]Department of Zoology, Institute for Coastal and Marine Research, Nelson Mandela University, Port Elizabeth, 6019, South Africa. [10]Greenland Climate Research Centre, Greenland Institute of Natural Resources, Kivioq 2, 3900 Nuuk, Greenland. [11]Zoophysiology, Department of Bioscience, Faculty of Science and Technology, Aarhus University, Aarhus 8000, Denmark. [12]Institute for Biodiversity and Ecosystem Dynamics – Freshwater and Marine Ecology, University of Amsterdam, 1090 GE Amsterdam, The Netherlands. [13]Royal Netherlands Institute for Sea Research, 1790 AB Den Burg, Texel, The Netherlands. [14]US National Oceanic and Atmospheric Administration, Office of National Marine Sanctuaries, Stellwagen Bank National Marine Sanctuary, Scituate, MA 02066, USA.

*Author for correspondence (wgough@stanford.edu)

W.T.G., 0000-0003-2701-5299; P.S.S., 0000-0002-2396-2670; D.E.C., 0000-0003-3641-1242; J.P., 0000-0002-8071-8340; F.E.F., 0000-0001-5973-3282; J.d.C., 0000-0003-0685-6750; A.S.F., 0000-0002-2822-233X; S.R.K.-R., 0000-0002-5208-1100; J.H.L., 0000-0002-9095-9770; G.P., 0000-0003-0545-7723; M.S.S., 0000-0002-7318-4977; S.K.A.V., 0000-0002-7563-2470; F.V., 0000-0003-1024-3244; J.A.G., 0000-0002-4170-7294

Received 29 March 2019; Accepted 24 September 2019

INTRODUCTION

For most animals, locomotion and maneuverability factor into critical life functions such as prey capture, predator avoidance and migratory success, and therefore can influence the margin between life and death (Dakin et al., 2018; Fish et al., 2003; Goldbogen et al., 2012; Hein et al., 2012; Williams et al., 2014). These locomotor functions manifest as complex maneuvers or behaviors that can be deconstructed into a series of simple elemental changes in body conformation, rotation or displacement (Full et al., 2002; Pennycuick, 1975; Segre et al., 2016, 2018; Webb, 1997). Many of these elements have evolved similarly among different taxa with distinct body plans as a result of common physical constraints or functional requirements (Donley et al., 2004). As a result, animals have evolved a wide range of convergent locomotor and maneuvering strategies across varying body sizes (Gleiss et al., 2011, 2017). Nowhere are the effects of scale more interesting than in the ocean, where release from gravitational constraints allows species with similar body plans and locomotory styles to range across several orders of magnitude in body mass, from the smallest fishes up to the blue whale (*Balaenoptera musculus*) (Motani, 2002; Pennycuick, 1992). Both toothed whales (Odontoceti) and baleen whales (Mysticeti) evolved gigantism after the evolutionary appearance of specialized foraging strategies (i.e. echolocation and filter feeding) that required the coupling of locomotion and feeding (Goldbogen and Madsen, 2018; Higham et al., 2016; Pyenson, 2017; Slater et al., 2017). However, what remains poorly understood is the influence of gigantism on the locomotor performance of whales and the ways in which it has enabled their foraging strategies and overall success as predators in a wide range of ocean ecosystems.

The body plans for cetaceans (whales and dolphins) typically consist of a fusiform body shape with appendages modified into streamlined flippers, fins and tails that oscillate or undulate to generate thrust, adjust attitude and help overcome drag (Fish and Lauder, 2006; Webb and De Buffrénil, 1990). At the largest scales, many large aquatic vertebrates (sharks, tuna, cetaceans) have evolved high aspect ratio lunate tails that are specialized for efficient locomotion and maneuvering (Bose and Lien, 1989; Dewar and Graham, 1994; Donley et al., 2004; Fish, 1998; Fish et al., 2014; Graham et al., 1990; Webb and De Buffrénil, 1990; Woodward et al., 2006). Paired, anteriorly placed flippers or fins are generally used as control surfaces to stabilize body trim or generate asymmetrical forces during turns, rolls or pitching motions (Fish and Lauder, 2017; Fish and Shannahan, 2000; Fish et al., 2006; Segre et al., 2016, 2018). Cetaceans (whales, dolphins and porpoises) include the largest animals that have ever lived (McClain et al., 2015), making them a unique and interesting organismal model to study the extremes of swimming performance.

Previous research on cetaceans has focused primarily on small, highly maneuverable toothed whales that can be studied in captivity

(Fish, 1993, 1998; Fish and Rohr, 1999; Fish et al., 2014, 2018; Rohr and Fish, 2004). In contrast, the logistical difficulties of working with larger baleen whales has made it more difficult to study the biomechanics and locomotion of these animals in the wild. As a result, much of the progress in this area has come about recently with the advent of archival, motion-sensing tags, which can be attached to wild animals for hours to days (Gleiss et al., 2011; Goldbogen et al., 2017; Martín López et al., 2016; Sato et al., 2007).

In considering the effects of scale on locomotion, previous studies have predicted that the oscillatory frequency of propulsive structures decreases in proportion to increasing body length (Hill, 1950; Pennycuick, 1992; Sato et al., 2007). Using simple muscle models, Hill (1950) predicted that the contraction speed of geometrically similar but differently sized muscles should scale inversely with their physical dimensions in order to balance the production of useful work and wasteful kinetic energy at a given movement speed. Accordingly, steady-state cruising by most vertebrates has been shown to occur in the 1–2 m s^{-1} range regardless of body size (Fish and Rohr, 1999; Sato et al., 2007; Watanabe et al., 2011). In contrast, dependence on body size has been shown to occur in other swimming performance measures such as maximum speed (Meyer-Vernet and Rospars, 2016; Shadwick and Gemballa, 2005; Wardle, 1975). Thus, the choice of movement speed for routine swimming may not reflect maximally achievable performance but instead relate to economy of transport (or the minimum cost of transport, COT_{min}) (Williams and Noren, 2009; Williams et al., 1993). However, recent research on free-ranging largemouth bass showed that swimmers exhibited slower speeds than their predicted COT_{min}, perhaps in order to balance competing functional demands such as prey capture (Han et al., 2017), suggesting that swimming performance is highly context dependent.

The hypothesis that stroke frequency is inversely correlated with body length is also supported by analyses of the dimensionless Strouhal number *St*, a ratio of the oscillatory frequency *f* and tailbeat amplitude *A* over swimming speed *U* [$St=(f \cdot A)/U$]. High propulsive efficiency occurs at $St \approx 0.25–0.35$ (Anderson et al., 1998; Rohr and Fish, 2004; Taylor et al., 2003; Triantafyllou et al., 1991). If swimming speed is constant and tailbeat amplitude scales isometrically with body length, then the oscillatory frequency must scale inversely with body length ($\sim L^{-1.0}$) in order to achieve optimal vortex generation (Fish, 1998; Pennycuick, 1992).

These size-dependent factors have played a major role in shaping the functional ecological theory of gigantic marine predators, but, until now, we have lacked the data for a comprehensive study on the kinematics of their oscillatory swimming. Specifically, it remains to be seen how swimming speed and oscillatory frequency scale with body length, particularly at the largest scale. To answer this question, we used tags with inertial sensors paired with unoccupied aerial system (UAS, or drones) imagery to quantify how key locomotor kinematics scale across a body length range of an order of magnitude, from morphologically similar Antarctic minke whales (~9 m; *Balaenoptera bonaerensis*, Burmeister 1867) to blue whales (~30 m) (Fig. 1). We used these data to test the hypothesis that stroke frequency decreases in inverse proportion with body length but instead found it scales to the approximate power of −0.5, while cruising speed remains near 2 m s^{-1} in order to minimize energy expenditure and thus is expected to be largely invariant with size (Sato et al., 2007; Watanabe et al., 2011, 2015).

MATERIALS AND METHODS

All procedures in the USA were conducted under approval of the National Marine Fisheries Service (Permits 781-1824, 16163, 14809, 16111, 19116, 15271, 20430), Canada DFO SARA/MML 2010-01/SARA-106B, National Marine Sanctuaries (MULTI-2017-007) and institutional IACUC committees. South Africa operations were conducted under approval from the Department of Environmental Affairs (Permit RES 2018/63) and Nelson Mandela University (Animal Ethics Approval A18-SCI-ICMR_001).

Tag data collection

We used multi-sensor suction-cup tags (Customized Animal Tracking Solutions, CATS; www.cats.is) to collect high sample rate kinematic and behavioral data from humpback whales (*Megaptera novaeangliae*, Borowski 1781), blue whales [*Balaenoptera musculus* (Linnaeus 1758)], fin whales [*Balaenoptera physalus* (Linnaeus 1758)], Bryde's whales (*Balaenoptera brydei*, Olsen 1913) and Antarctic minke whales (*Balaenoptera bonaerensis*, Burmeister 1867). Each tag included tri-axial accelerometers, magnetometers and gyroscopes sampling at 40–400 Hz, and pressure sensors sampling at 10 Hz. Pressure and high sample rate accelerometer data recorded by the tag allowed estimation of swimming speed using the root-mean-square (RMS) amplitude of tag vibrations (Cade et al.,

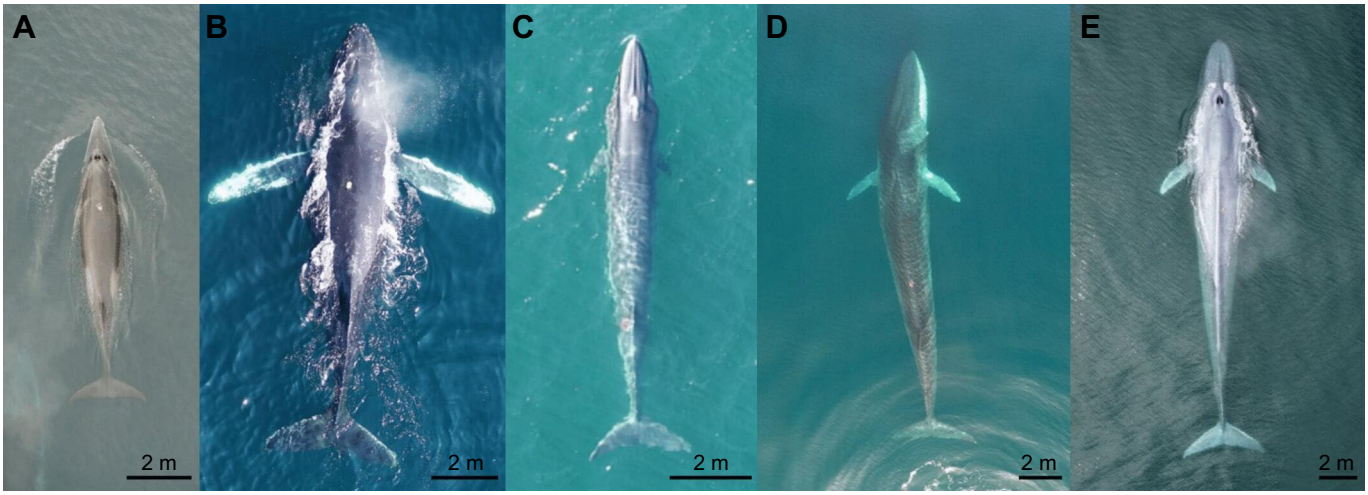

Fig. 1. Representative overhead unoccupied aerial system (UAS) photographs and scale bars for each study species. (A) Minke, (B) humpback, (C) Bryde's, (D) fin and (E) blue whale.

2018). Tag sensors were rotated into whale-body frame orientation, and animal pitch, roll and heading were derived (Cade et al., 2016; Johnson and Tyack, 2003). Cameras collected video at 30 frames s^{-1} and were integrated into the tags in different orientations: (1) forward along the mid-line axis of the tag, (2) offset at ∼45 deg from the mid-line axis, and (3) forward and backward along the mid-line axis. Additional information about tag design and deployment can be found in Cade et al. (2016). Tag deployments occurred on whales from July 2014 to October 2018 in a wide range of geographic locations including the Antarctic Peninsula for *B. bonaerensis*, the Azores, Portugal, for *B. physalus* and *B. musculus*, Eastern Greenland for *B. physalus* and *M. novaeangliae*, Monterey Bay, USA, for *B. physalus*, *B. musculus* and *M. novaeangliae*, Plettenburg Bay, South Africa, for *B. brydei*, Santa Barbara Channel, USA, for *B. musculus* and *M. novaeangliae*, and Stellwagen Bank, USA, for *M. novaeangliae* (Table S1).

Whale photogrammetry and morphometrics

We collected high-resolution aerial images via UAS between 2017 and 2018 (Fig. 1). Nadir images of whales were collected during a subset of tag deployments for *B. bonaerensis* (Antarctic Peninsula), *M. novaeangliae* (Antarctic Peninsula, Eastern Greenland, Monterey Bay and Santa Barbara Channel), *B. brydei* (Plettenburg Bay), *B. physalus* (Azores, Eastern Greenland, Monterey Bay) and *B. musculus* (Monterey Bay, Santa Barbara Channel, Azores). Specifically, we used a DJI Phantom 3 Professional quadcopter, a DJI Phantom 4 Pro quadcopter, and two types of hexacopters, the FreeFly Alta 6 and a custom Mikrokopter-based LemHex-44. The Phantom 3 Professional quadcopter was fitted with a Sony EXMOR 1/2.3 inch camera, 4000×3000 pixel resolution and a 94 deg field of view. The Phantom 4 Pro quadcopter was fitted with a 1 inch CMOS camera sensor, 5472×3078 pixel resolution and an 84 deg field of view. Both hexacopters were fitted with a Lightware SF11/C laser altimeter and a Sony Alpha A5100 camera with an APS-C (23.5×15.6 mm) sensor, 6000×4000 pixel resolution and either a Sony SEL50 50 mm or SEL35 35 mm focal length low distortion lens. The laser altimeter and cameras were co-located on a 2-axis gimbal with pitch angle controlled via remote control to aid in positioning and ensure image collection at the nadir. Measurement error for both quadcopters was calculated as <1.10% by Putch (2017). Measurement error for both hexacopters was calculated by measuring an object of known size placed in the water (i.e. a paddle) at various altitudes. The Alta 6 had a measurement error of <0.30%, while the LemHex-44 measurement error was <1.50%. We used similar methods for hand launch and recovery from small boats to those described in Durban et al. (2015), with the addition of a first-person view (FPV) screen attached to each flight controller, giving the pilot a live feed from the photogrammetry camera. The LemHex-44 required a single operator where the pilot manually controlled the gimbal and camera's shutter, whereas the Alta 6 required two operators, a pilot and camera operator. We collected images in bursts (LemHex-44 and Alta 6) or on a 2 s timer (Phantom 3, Phantom 4) with the whale in full frame lengthwise with a high shutter rate of 6 frames s^{-1} as the animal surfaced or was just below the surface (Fig. 1).

We manually selected UAS images for measuring the total length and maximum diameter of individual whales if the lower jaw, fluke notch and sides were clearly visible and if the animal appeared straight with minimum curvature at the surface or just below. We measured total length from the tip of the lower jaw to the fluke notch and manually selected maximum diameter as the widest width of the whale posterior of the axilla. We performed all measurements using ImageJ 1.5i (Schindelin et al., 2012). We used the segmented or straight-line tool to draw a line from the tip of the lower jaw to the fluke notch, or from each side at the widest width, to measure the distance in number of pixels. We calculated total length and maximum diameter using an approach similar to Fearnbach et al. (2012), where the number of pixels was multiplied by the ground sampling distance (GSD):

$$L = n_{\text{pixels}} \times \text{GSD}, \tag{1}$$

$$\text{GSD} = \left(\frac{a}{l_{\text{focal}}}\right)\left(\frac{w_{\text{S}}}{w_{\text{p}}}\right), \tag{2}$$

where L is the total length of the animal (m), n_{pixels} is the number of pixels, a is altitude (m), l_{focal} is focal length (mm), w_{S} is the width of the sensor (mm) and w_{p} is the width of the image resolution (pixels). The width was used for the sensor size and image resolution because the whales were captured full frame widthwise.

Tailbeat measurement

We chose the transverse axis of the gyroscope signal to quantify rotational body movements along the pitch axis of the animal. This improved upon previous studies (Martin López et al., 2015, 2016) which relied on the longitudinal axis of the accelerometer because it allowed us to disregard the orientation of the body and it was highly effective during high pitch angle segments that would otherwise be prone to gimbal lock. For 5 out of 143 deployments, we relied on the longitudinal axis accelerometer method with a high-pass filter because of malfunctioning gyroscope signals. We compared gyroscope and accelerometer signals from the same deployment to quantify uncertainties and ensure that slight differences would not affect our results. For each deployment, we calculated the average value for the oscillatory signal, then used a customized Matlab script to identify full tailbeats, here defined as one consecutive upstroke and downstroke, using a zero-crossing method. We set a consistent and conservative series of thresholds aimed at ignoring incomplete or asymmetrical tailbeats in the data sets. To be included in our analyses, a tailbeat had to have a period measured at less than 10 s, feature exactly two peaks (one upstroke and one downstroke), with a magnitude towards either the upstroke or downstroke being less than 15 times the magnitude in the other direction. We visually inspected the resultant tailbeats to confirm that our thresholds were performing correctly. We removed deployments from subsequent analyses if they identified fewer than 200 full tailbeats (Table 1). We calculated multiple time-synchronized kinematic and behavioral parameters for the duration of each full tailbeat (Fig. 2) including the oscillatory frequency, f, as 1/period, the average swimming speed (Cade et al., 2018), the average depth and the modal behavioral state (described below).

Measurement of speed

Measurement of the swim speed relied on turbulent flow to vibrate the tag and, as a result, could not resolve speeds below ∼1 m s^{-1} (Cade et al., 2018). For each deployment, we regressed the oscillatory frequency of each individual tailbeat period against the average speed during that stroke. To ensure that our regressions were accurately capturing the relationship between oscillatory frequency and swimming speed, we only included tailbeat periods with an average speed higher than one standard deviation above the lowest recorded speed. So as not to bias results with artificially high minimum speeds as a result of the method's low-speed threshold, we used median swimming speed values for comparative analyses among species.

Journal of Experimental Biology (2019) 222, jeb204172. doi:10.1242/jeb.204172

Table 1. Metadata related to each included species

	No. of individuals	Average stroke count	Average frequency (Hz)	Median swim speed (m s^{-1})	% Time			Average length (m)	Fineness ratio	Average U_{opt} (m s^{-1})
					Descending	Ascending	Bottom			
All whales										
Minke	7	4699±2100	0.365±0.029	2.25±0.23	12.8±4.58	12.2±3.89	25.0±12.4	–	–	–
Humpback	97	1933±1796	0.229±0.039	1.77±0.41	16.6±4.62	17.5±5.20	22.0±11.6	–	–	–
Bryde's	5	1398±592	0.254±0.033	1.91±0.46	11.2±4.95	11.9±5.84	25.9±8.75	–	–	–
Fin	7	1591±2086	0.217±0.037	2.27±0.72	11.2±2.51	11.3±4.99	35.1±12.8	–	–	–
Blue	27	1370±957	0.190±0.016	2.11±0.41	14.8±4.63	17.2±3.43	41.3±9.97	–	–	–
With UAS										
Minke	2	4201±4415	0.360±0.009	2.30±0.04	–	–	–	8.33±0.41	5.64–5.97	1.80±0.00
Humpback	31	2319±2288	0.246±0.038	1.99±0.45	–	–	–	11.09±1.81	4.13–5.74	1.95±0.04
Bryde's	2	972±261	0.254±0.012	1.65±0.64	–	–	–	12.04±2.92	–	–
Fin	5	1982±2416	0.212±0.041	2.40±0.52	–	–	–	18.65±0.79	7.52–10.2	1.92±0.03
Blue	20	1412±991	0.187±0.016	2.08±0.46	–	–	–	22.59±1.36	6.86–8.74	2.05±0.03

A distinction is shown between our full (All whales, n=143) and with-morphometrics datasets (With UAS, n=60). Certain variables were not calculated for both datasets. All values are given as means±s.d. except for fineness ratio, which is given as a range from minimum to maximum values. U_{opt}, optimal swimming speed.

Modeling optimal speed

We combined measurements of body total length and maximum diameter with a simple model of non-feeding transport to predict the swimming speed associated with the minimum energetic cost of transport (Weihs, 1973). The modeling starts with estimating the (metabolic) energy expended (ε; J) to travel a given distance (d) as

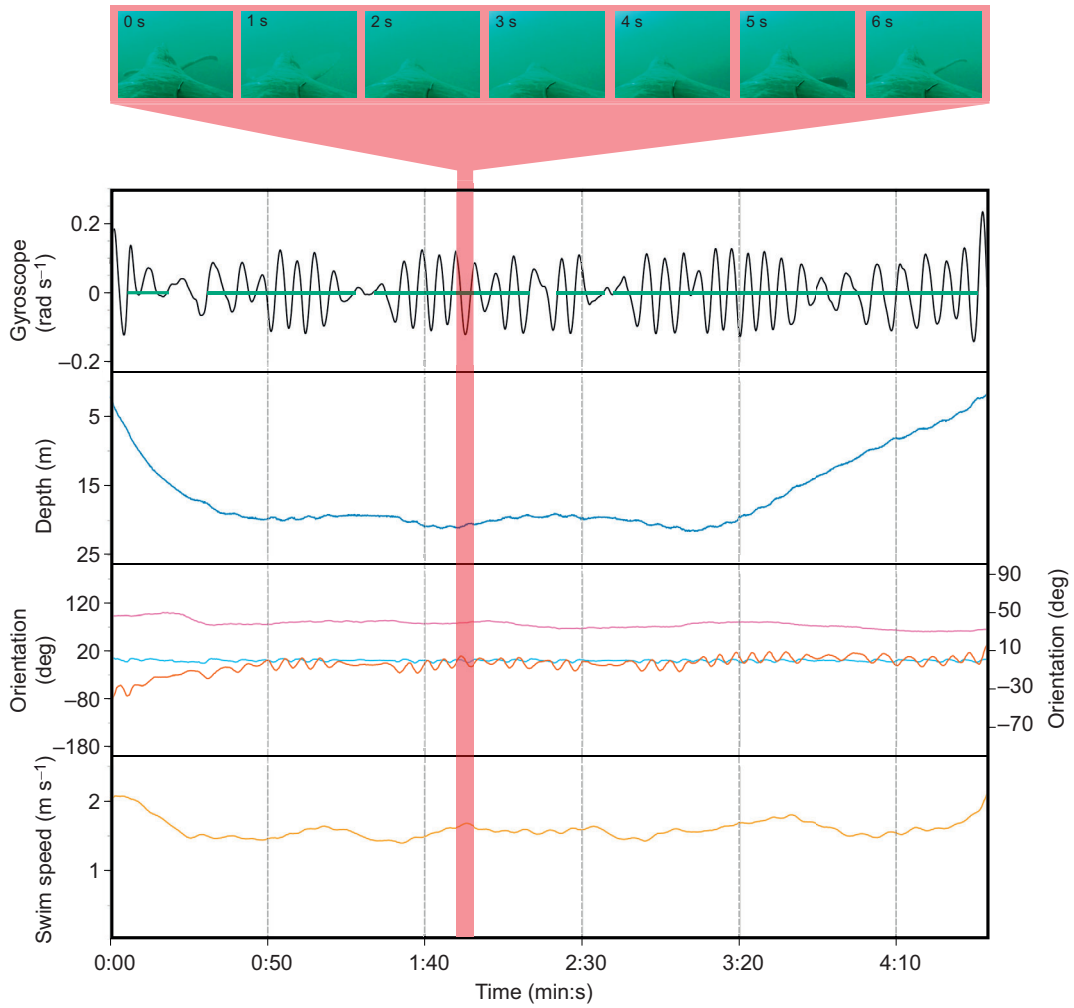

Fig. 2. Section of CATS tag data showing time-synced data streams. The video stills are faced caudally from a common reference point and illustrate a single tailbeat cycle. These stills are correlated in time with the vertical red bar intersecting each data stream. The green horizontal lines at the zero line of the first data stream (Gyroscope) correspond to symmetrical tailbeats that fit our detection thresholds and were included in our analyses. The three lines in the third data stream (Orientation) correspond to pitch (right y-axis; orange), roll (left y-axis; pink) and heading (left y-axis; blue) changes.

follows:

$$\varepsilon = \left[\mathrm{BMR}\left(\frac{d}{U}\right)\right] + \left[U^2\left(\frac{(1/2)\rho S C_\mathrm{d} d\lambda}{\eta_\mathrm{m}\eta_\mathrm{p}}\right)\right]. \quad (3)$$

The second term corresponds to the energy expended by the locomotor musculature to compensate for the drag produced (as propulsive drag equals drag in this instance). Here, d is the distance traveled (set to 1 body length), U is the swimming speed (m s^{-1}), ρ is the density of seawater (=1025 kg m^{-3}), S is the wetted surface area (m^2) of the animal calculated using coefficients from computational fluid dynamics modeling or literature sources for each included species (Bose and Lien, 1989; Kermack, 1948; Parry, 1949), C_d is the dimensionless drag coefficient of the body in a rigid configuration (~0.002–0.005) (Kooyman, 1989), λ is the drag correction due to the heaving body and caudal tail (~2–3) (Fish, 1993, 1998), η_m is the (dimensionless) metabolic efficiency and η_p is the (dimensionless) propulsive efficiency. Both of the efficiency terms are considered to be constant across body size ranges (Fish, 1996, 2001; Fish and Rohr, 1999). The first term in Eqn 3 accounts for the energy expenditure by the organ and tissue in the rest of the body, which here is estimated by the Kleiber (1975) basal metabolic rate (BMR) correlation, corrected by a factor of 1.6, that is based upon previous estimates of swimming or dive recovery metabolic rates (Costa and Williams, 1999; Lockyer, 1981; Scholander, 1940) and accounts for a higher level of metabolic activity during active swimming over long durations:

$$\mathrm{BMR} = 6.56m^{0.75}, \quad (4)$$

where m is body mass (kg). The model yields an optimal swimming speed (U_opt) for which a minimum of energy stored in the body is used to cover distance d (Weihs, 1973):

$$U_\mathrm{opt} = \left(\frac{\mathrm{BMR}\eta_\mathrm{m}\eta_\mathrm{p}}{\lambda\rho\, S C_\mathrm{d}}\right)^{0.33}. \quad (5)$$

Tail-attached tag measurements

As for fish swimming in the wild (Han et al., 2017; Watanabe et al., 2019), stroke amplitude is difficult to measure in tagged cetaceans (van der Hoop et al., 2017). However, during a single humpback whale deployment in 2017, the tag slipped from its original placement on the back of the animal (between the dorsal fin and blowhole) and attached to the dorsal aspect of the tail near the right fluke-blade midline. As shown in Fig. 3, the tag was aimed anteriorly towards the body and remained so for 68 min. Such a fortuitous event allowed us to measure the tailbeat amplitude as a local, short-duration change in depth from the tag's pressure transducer. We included sequences with at least three tailbeats that had an overall depth change near zero (n=14). For each sequence, we calculated the midline – from the midpoint of the first tailbeat to the midpoint of the final tailbeat – and then averaged the distance from that midpoint to the top of each upstroke and to the bottom of each downstroke (Fig. 3 inset). For these same tailbeat sequences, we measured the oscillatory frequency and swimming speed, and estimated the Strouhal number for each sequence.

Comparison with two simple oscillatory models

We used a derivation of the Strouhal number equation to estimate the oscillatory frequency of an optimally oscillating vortex generator:

$$f = \frac{USt}{A}, \quad (6)$$

with U set at 2 (m s^{-1}) based upon the average speeds in our observed dataset, St set at 0.3 to simulate optimality and A set at one-fifth of body length (Bainbridge, 1958; Fish and Rohr, 1999; Rohr and Fish, 2004). We applied this model over a 10–20 m range of total body lengths to facilitate a direct comparison with our observed dataset.

An alternative to Strouhal number scaling is the idea that, to sustain a form of low-cost swimming, the oscillatory frequency is set to the resonant frequency of the caudal tail, here seen as a driven and damped oscillator (Ahlborn et al., 2009; Hamilton et al., 2004; Pabst, 1996, 2000). In this model, drag provides the damping, the tail musculature provides the driving force, and the sub-dermal sheath and blubber surrounding the tail stock acts as the spring-like oscillatory restoring force. Swimming near the 'optimal' oscillatory frequency means that the driving force will be set at the oscillatory frequency that generates the greatest tailbeat amplitude. In low-damping conditions, this oscillatory frequency will coincide with the so-called 'natural' frequency of the tail tissue and bone under the sole influence of the spring-like restoring force provided by the sub-dermal sheath (Kreyszig, 2016). With the sub-dermal sheath forces acting like a cantilever beam oscillating in seawater, the oscillatory

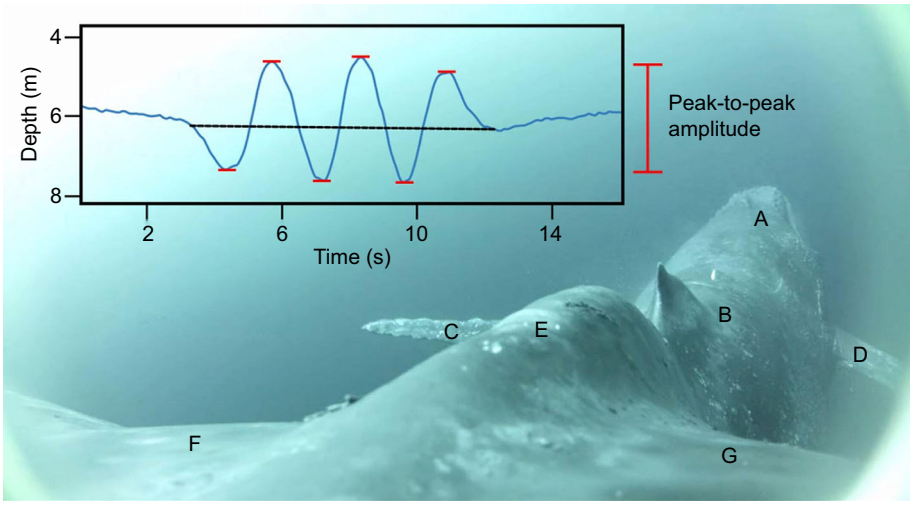

Fig. 3. Tailbeat amplitude measurement. A video still from the deployment of interest. (A) Rostrum, (B) dorsal fin, (C) left flipper, (D) right flipper, (E) peduncle, (F) left fluke blade and (G) right fluke blade. The inset is a schematic diagram of our peak-to-peak amplitude measurement method.

Journal of Experimental Biology (2019) 222, jeb204172. doi:10.1242/jeb.204172

frequency would thus be modeled as:

$$f = \frac{\pi}{2}\sqrt{\frac{3EI}{2m_e L_{os}^3}}, \quad (7)$$

where E parameterizes the effective Young's modulus of cetacean tissue (approximated as 2 MPa from Long et al., 2002), I is the second moment of area (m^4) and m_e is the effective mass (kg) of the beam (Denny, 1988); we doubled that effective mass to account for the added mass of the body accelerating in a fluid (Lighthill, 1970; Webb, 1975). Here, the model assumed that the cranial 40% of body length was stationary during oscillation, with the caudal 60% of body length oscillating (L_{os}). We applied this model over the same 10–20 m range of total body lengths as our Strouhal model.

Statistical analyses

The datasets supporting this article are available from the corresponding author on request. We performed all statistical analyses using R (version 3.4.1, package nlme) with a significance level of 0.05. For each analysis, continuous variables (total length, oscillatory frequency, median cruising speed, coefficient of variation) were $\log_{10}$ transformed before inclusion as predictors or response variables to normalize our data and conform to the basic model of scaling as a power function. For the subset of deployments with morphometric measurements (n=55), we created a linear mixed-effects model with body length as the predictor, the mean oscillatory frequency of a deployment as the response and species as a random effect. The results of this model were used to determine the regression line and standard error of the mean for our comparison of body length and oscillatory frequency. Next, we created a linear mixed-effects model with body length as the predictor, the coefficient of variation for the oscillatory frequency of a deployment as the response and species as a random effect. Finally, we created a linear mixed-effects model with body length as the predictor, median swimming speed as the response and species as a random effect.

We used our complete dataset to create a linear mixed model comparing the oscillatory frequency between dive descent and dive ascent stages across all species. The model included species and individuals within species as random effects. We also performed identical analyses on a species-specific basis for *B. bonaerensis*, *M. novaeangliae* and *B. musculus*. These models included individuals within species as a random effect. Our final models included swimming phase as the predictor, coefficient of variation for the oscillatory frequency of a deployment as the response and species as a random effect.

RESULTS

Variation in oscillatory kinematics

Metadata and summary statistics for tagged whales (n=143 total, n=60 with UAS-measured morphometrics) are shown in Table 1. The number of tailbeats in a deployment ranged from 260 to 9458 with a mean (±s.d.) of 1927±1784. Swim speeds ranged up to 8.28 m s^{-1} (lower bound was unresolved) with a median of 1.89±0.038 (median±standard error) and oscillatory frequencies ranged from 0.10 to 1.00 Hz with a mean (±s.e.m.) of 0.23±0.004 Hz (Fig. 4). Swim speed increased with an increase in oscillatory frequency in all species (Fig. 5). For all species combined, we calculated a single regression equation of swim speed on oscillatory frequency ($\hat{y}$=0.54x−0.80; R^2=0.24). For the lone humpback whale tail-attached deployment, we found the mean (±s.d.) tailbeat amplitude (2.63±0.79 m), oscillatory frequency (0.25±0.06 m), swimming speed (2.61±0.25 m) and Strouhal number (0.24±0.04).

Effect of body length on oscillatory frequency and swimming speed

Fig. 6 compares the tag-based measurements of the heaving frequency with predictions from optimal Strouhal scaling (Eqn 6) and oscillating beam models (Eqn 7). The same figure also shows a comparison between measurements of steady-state swimming speed and the predicted optimal speed as per Eqn 5. There was a clear decrease in oscillatory frequency (f_{obs}) with increasing total length in both an intraspecific and interspecific context, but no relationship between cruising speed and total length (Table 1). The regression for observed speed (U_{obs}) corresponded very closely with the regression for optimal speed (U_{opt}) (Table 2). Overall, the measured

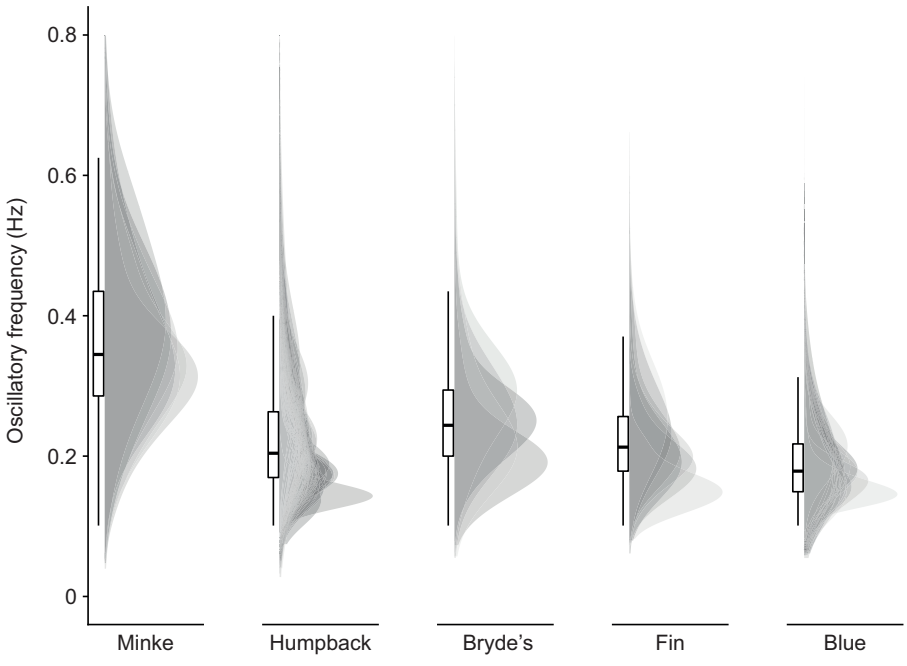

Fig. 4. Density distributions of the oscillatory frequency calculated for each included tailbeat for a single whale. Distributions have been grouped by species. The box plots show the mean, 25% and 75% percentiles, and whiskers moving out to the farthest outliers.

Journal of Experimental Biology (2019) 222, jeb204172. doi:10.1242/jeb.204172

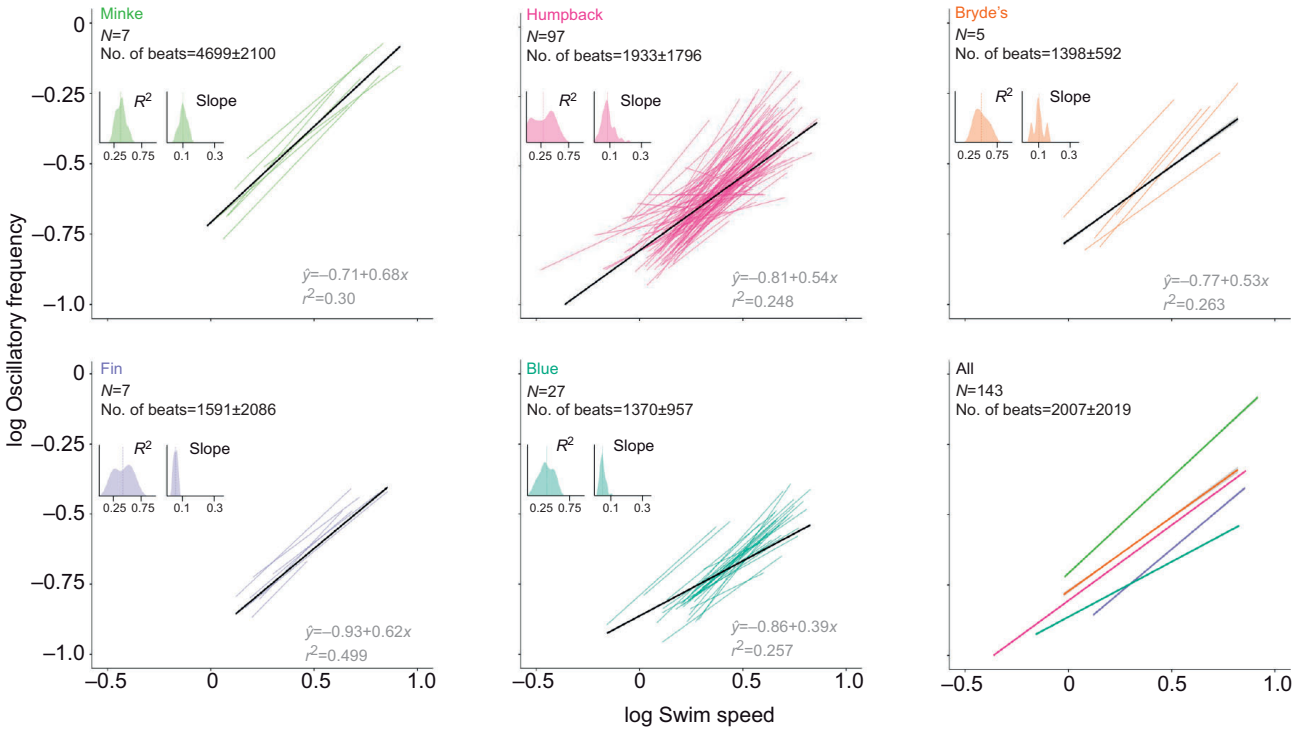

Fig. 5. Regression between the oscillatory frequency (Hz) and average speed (m s^{-1}) of each whale. Individuals of each species are represented by the colored regression lines. The black regression lines are the averages for each species. In the 'All' plot (bottom right), each of the species-averaged regression lines is matched to the initial line color chosen for that species. The number of individuals (*N*) and the mean (±s.d.) number of tailbeats is shown in each panel. Additional information (R^2 and slope) is given in the form of density distributions grouped by species.

swimming speed followed the insensitivity to body length exhibited by the model. However, the scaling of our oscillatory frequency data $f \approx L^{-0.5}$ does not agree with the $f \approx L^{-1.0}$ trend suggested by both the *St* and oscillating cantilever models.

More specifically, we found a significant dependence on total body length in the mean oscillatory frequency for an individual whale of any species (d.f.=54; $t=-6.69$; $P<0.001$). The effect of total length on the coefficient of variation of the oscillatory frequency for an individual whale was not significant (d.f.=54; $t=-0.62$; $P=0.54$) and, similarly, the effect of total length on the median cruising speed for an individual whale was not significant (d.f.=54; $t=0.90$; $P=0.37$).

DISCUSSION

The scale dependence of locomotor performance

Our measurements from baleen whales of varying body lengths indicate that while oscillatory frequency decreases with body length to the power of −0.53, cruising speed is largely invariant with body length (to the power of 0.08). These results are broadly consistent with previous studies for other swimming animals (Sato et al., 2007), particularly endotherms (Watanabe et al., 2015). The empirically derived oscillatory frequencies and cruising speeds found in our investigation can inform studies attempting to model these kinematic parameters across wide body length ranges (Alexander, 2005; Vogel, 2008). Many studies have included inexact measurements for large swimming animals or excluded them completely from the modeling (Bejan and Marden, 2006; Gazzola et al., 2014). The model put forth by Gazzola et al. (2014) includes an average blue whale cruising speed of 6 m s^{-1} and a resulting oscillatory frequency of 0.36 Hz. These values are roughly triple what we found in the present study using empirical data for the same species performing natural behaviors.

Our observed scaling exponent of −0.53, derived by least-squares regression of *f* onto *L*, differs from that predicted by the two simple scaling models. The cantilevered beam model (Eqn 7) – taking as inputs constant values of *E* and *I*, and variable values of *L* and *M* – predicts a scaling exponent of −1, nearly double what we observed. We obtained the same exponent, −1, in the Strouhal model, which takes as inputs a constant speed (2 m s^{-1}), constant Strouhal number (0.3) and the variable *L*. The fact that the observed exponent differs from the predicted suggests that these whales are not operating as simple cantilevered beams or as optimally oscillating vortex generators. The cantilevered beam model lacks damping forces that would reduce the predicted exponent. The Strouhal model assumes optimal fluking based on efficient vortex shedding and interaction. The apparent failure of these models points us toward appropriate ways to complicate subsequent models through added damping or relaxation of optimality constraints.

Our results corroborate previous controlled studies and lend support for a set of hydrodynamic principles governing the locomotion of free-swimming animals down to the level of an individual stroke (Bainbridge, 1958; Fish, 1998; Kohannim and Iwasaki, 2014). The difficulty of obtaining stroke amplitude measures for our study animals is a limitation that precludes the type of precise hydrodynamic analysis found in previous studies, but the stroke amplitude determined from the tail-attached deployment corresponds well with previous estimates of stroke amplitude as one-fifth of body length (Bainbridge, 1958; Fish and Rohr, 1999; Rohr and Fish, 2004). Although we lacked UAS-based measures of the tail-attached animal, a calculation for our average amplitude measure of 2.37 m suggests a total body length of 11.85 m. For comparison, the mean (±s.d.) body length for humpback whales within our dataset was 11.09±1.81 m. Previous studies have shown amplitude to be invariant with changes in

Journal of Experimental Biology (2019) 222, jeb204172. doi:10.1242/jeb.204172

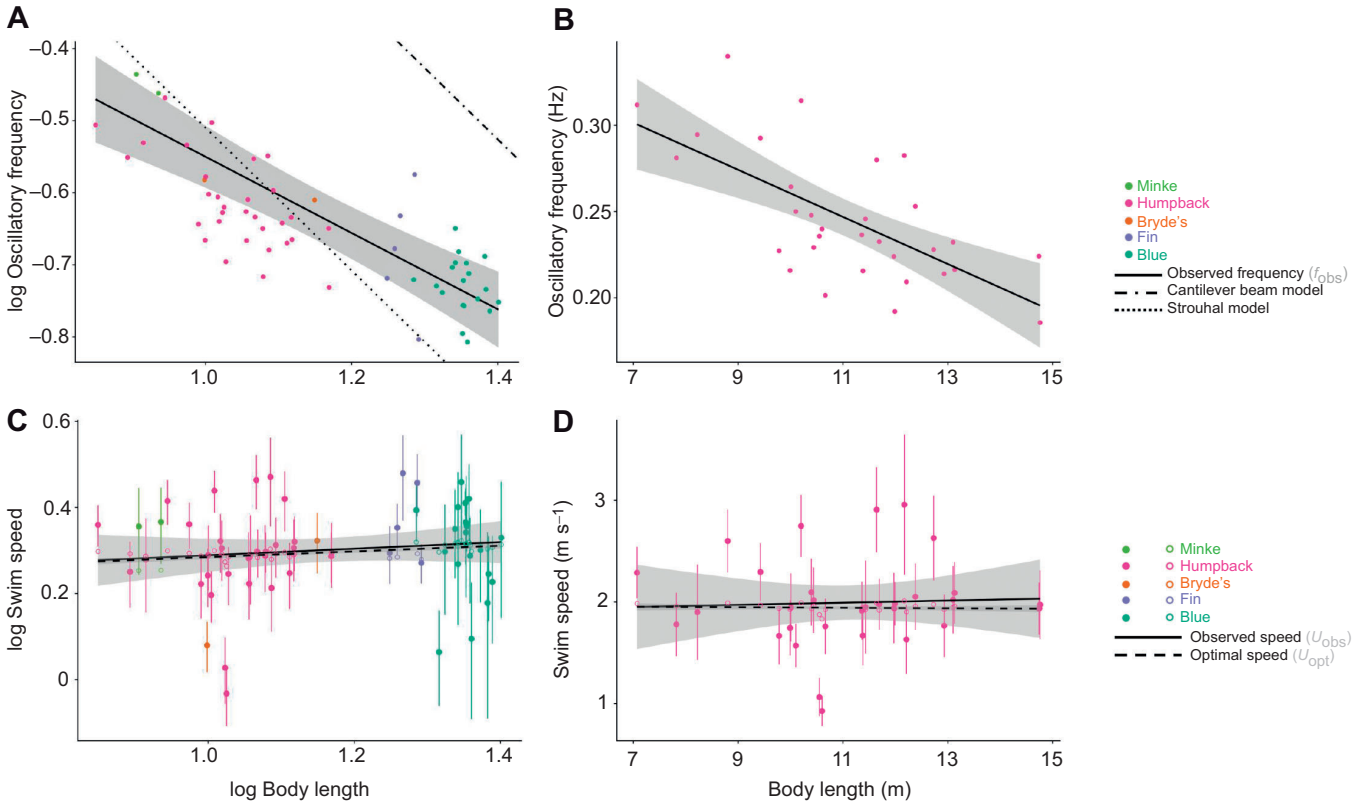

Fig. 6. Relationships between body length and both oscillatory frequency and cruising speed. (A) Interspecific log-transformed mean oscillatory frequency (Hz) for all species. (B) Intraspecific humpback mean oscillatory frequency. (C) Interspecific log-transformed median cruising speed (m s^{-1}) for all species. (D) Intraspecific humpback median cruising speed. Solid lines denote the observed regressions and gray shading represents the standard error. We calculated the regression for A using our linear mixed model with species as a random effect. The dot-dash and dotted lines represent the regressions for our cantilever beam and Strouhal models, respectively. The open circles shown in C represent the modeled U_{opt} values for each whale. For each point in C and D, a single vertical line extends from the 25th percentile (bottom of the line) to the 75th percentile (top of the line), with the point in the middle denoting the median.

forward speed, so the lack of amplitude measures for each stroke does not considerably lessen our understanding of the animal's overall hydrodynamic scope (Bainbridge, 1958; Fish, 1998; Kohannim and Iwasaki, 2014). Using the tail-attached deployment, we also obtained the first empirical measurements of Strouhal number for a large cetacean. These values fall near the predicted range of $St \approx 0.25–0.35$ that has been shown to correspond to high hydrodynamic efficiency (Anderson et al., 1998; Rohr and Fish, 2004; Taylor et al., 2003; Triantafyllou et al., 1991). Throughout the duration of this deployment, the animal transited (moved steadily from one location to another) and performed a single feeding lunge. Of all the behaviors performed by animals in our dataset, transiting is most similar to the steady-state swimming performed by animals in controlled, laboratory and aquarium studies (Bainbridge, 1958; Fish and Rohr, 1999; Fish et al., 2014). This could explain why the Strouhal number for this individual fell so close to the theoretical optimum.

Table 2. Equations and R^2 values calculated for each regression shown in Fig. 6

	Equation	R^2 value
Oscillatory frequency		
All species observed	$\hat{y}=-0.53x-0.02$	0.635
Humpback observed	$\hat{y}=-0.58x-0.01$	0.444
Strouhal model	$\hat{y}=-1.0x+0.48$	–
Cantilever beam model	$\hat{y}=-1.0x+0.86$	–
Swim speed		
All species observed	$\hat{y}=0.08x+0.21$	0.013
All species optimum	$\hat{y}=0.07x+0.22$	0.476
Humpback observed	$\hat{y}=0.05x+0.23$	0.001
Humpback optimum	$\hat{y}=-0.02x+0.31$	0.030

The R^2 values for the Strouhal and cantilever beam models were approximately 1 and, therefore, were not included.

One of the common methods used to quantify the efficiency of locomotor modes is calculating the cost of transport over a set distance, either as a mass-specific or as an objective estimation (Alexander, 1999; Schmidt-Nielsen, 1972; Watanabe et al., 2011; Williams, 1999; Williams et al., 2014). Calculation of the cost of transport typically requires an estimate of metabolic rate using oxygen consumption or some other metric of metabolism (Schmidt-Nielsen, 1972; Sumich, 1983; Williams, 1999; Williams et al., 1993). Here, from first principles we predicted the forward speed at which the energetic cost of transport is minimized. This is a common optimization estimate and can be useful as a comparison against measured speed (Alexander, 1999; Watanabe et al., 2011). The results of our modeled optimum speed agree with previous research showing that the preferred speed of many endothermic swimmers is 1–2 m s^{-1} (Sato et al., 2007; Watanabe et al., 2011, 2015). The slight increase in observed swimming speed above our modeled values could be due to increased behavioral variation throughout the course of the deployment. Our optimum swimming speed equation assumes that an animal is in a steady-state, non-feeding locomotor mode. Conversely, our observed values include

maneuvers and non-steady swimming related to feeding or other ecologically relevant functions, many of which are being performed above typical cruising speeds (Cade et al., 2016; Goldbogen et al., 2006, 2011, 2012; Simon et al., 2012). Han et al. (2017) performed a similar comparison between optimal and observed swimming speeds in largemouth bass (*Micropterus salmoides*) and found the opposite result. Bass routinely swam slower than their predicted optimum for cost of transport. It was suggested by Han et al. (2017) that other considerations may be prioritized in the wild for largemouth bass, such as the need for slower speeds in order to efficiently detect and capture food.

Conclusion

Our study is the first to quantify the kinematics of free-swimming baleen whales over an order of magnitude in body length. Our results for oscillatory frequency and cruising speed are more accurate than previous models and show that, while oscillatory frequency decreases with increasing body length, cruising speed remains largely invariant. A model predicting the optimal swimming speed aligned closely with the cruising speeds observed in our study animals. Models predicated on Strouhal number and an oscillating cantilever beam could not predict the full variation in oscillatory frequency within our dataset, but a small number of empirical measurements of the Strouhal number fell within the range for high hydrodynamic efficiency. Major deviations from theory may reflect the competing demands for different locomotor functions during common behaviors such as foraging.

Acknowledgements

Our fieldwork efforts would not have been successful without our boat crew and logistics personnel. Dr Nikolai Liebsch and Dr Peter Kraft from Customized Animal Tracking Solutions have been instrumental in the design and maintenance of our inertial sensing tags. Xitlaali Castellanos performed the Strouhal measurements for the humpback tail-attached deployment. Dr Robin Elahi assisted with the design and implementation of our statistical analyses.

Competing interests

The authors declare no competing or financial interests.

Author contributions

Conceptualization: W.T.G., P.S.S., D.E.C., J.P., F.E.F., A.S.F., J.H.L., M.S.S., J.A.G.; Methodology: W.T.G., P.S.S., K.C.B., D.E.C., J.P., F.E.F., A.S.F., J.K., J.H.L., M.S.S., J.A.G.; Software: W.T.G., D.E.C., J.K.; Formal analysis: W.T.G., K.C.B., J.P., J.K.; Investigation: W.T.G., P.S.S., K.C.B., D.E.C., J.P., F.E.F., J.D., J.d.C., A.S.F., D.W.J., S.R.K.-R., M.O., G.P., M.S.S., M.S., S.K.V., F.V., D.N.W., J.A.G.; Resources: K.C.B., D.E.C., J.P., J.D., J.d.C., A.S.F., D.W.J., J.K., M.O., G.P., M.S., S.K.A.V., F.V., D.N.W., J.A.G.; Data curation: W.T.G., P.S.S., K.C.B., D.E.C., J.D., A.S.F., D.W.J., S.R.K.-R., J.K., M.O., G.P., M.S.S., M.S., S.K.A.V., F.V., D.N.W.; Writing - original draft: W.T.G.; Writing - review & editing: W.T.G., P.S.S., K.C.B., D.E.C., J.P., F.E.F., J.D., J.d.C., A.S.F., D.W.J., S.R.K.-R., J.K., J.H.L., M.O., G.P., M.S.S., M.S., S.K.A.V., F.V., D.N.W., J.A.G.; Visualization: W.T.G., M.S.S., J.A.G.; Supervision: J.P., F.E.F., A.S.F., J.H.L., M.S.S., J.A.G.; Project administration: A.S.F., J.A.G.; Funding acquisition: J.P., F.E.F., A.S.F., J.A.G.

Funding

This research was funded in part by grants from the National Science Foundation (IOS-1656691, IOS-1656676, IOS-1656656; OPP-1644209), the Office of Naval Research (N000141612477), a Terman Fellowship from Stanford University, and a National Science Foundation INSPIRE Special Projects grant (1344227). Additional Monterey Bay CATS tag deployments were funded by grants from the American Cetacean Society Monterey and San Francisco Bay chapters, and by the Meyers Trust. Bryde's whale tagging operations in South Africa were funded by the Percy Sladen Memorial Fund, PADI Foundation, Torben and Alice Frimodts Fund, and Society for Marine Mammology.

Supplementary information

Supplementary information available online at
http://jeb.biologists.org/lookup/doi/10.1242/jeb.204172.supplemental

References

Ahlborn, B. K., Blake, R. W. and Chan, K. H. S. (2009). Optimal fineness ratio for minimum drag in large whales. *Can. J. Zool.* **87**, 124-131. doi:10.1139/Z08-144

Alexander, R. M. (1999). *Energy for Animal Life*. OUP Oxford.

Alexander, R. M. (2005). Models and the scaling of energy costs for locomotion. *J. Exp. Biol.* **208**, 1645-1652. doi:10.1242/jeb.01484

Anderson, J. M., Streitlien, K., Barrett, D. S. and Triantafyllou, M. S. (1998). Oscillating foils of high propulsive efficiency. *J. Fluid Mech.* **360**, 41-72. doi:10.1017/S0022112097008392

Bainbridge, R. (1958). The speed of swimming of fish as related to size and to the frequency and amplitude of the tail beat. *J. Exp. Biol.* **25**, 109-133.

Bejan, A. and Marden, J. H. (2006). Unifying constructal theory for scale effects in running, swimming and flying. *J. Exp. Biol.* **209**, 238-248. doi:10.1242/jeb.01974

Bose, N. and Lien, J. (1989). Propulsion of a fin whale (Balaenoptera physalus): why the fin whale is a fast swimmer. *Proc. R. Soc. Lond. B Biol. Sci.* **237**, 175-200. doi:10.1098/rspb.1989.0043

Cade, D. E., Friedlaender, A. S., Calambokidis, J. and Goldbogen, J. A. (2016). Kinematic diversity in rorqual whale feeding mechanisms. *Curr. Biol.* **26**, 2617-2624. doi:10.1016/j.cub.2016.07.037

Cade, D. E., Barr, K. R., Calambokidis, J., Friedlaender, A. S. and Goldbogen, J. A. (2018). Determining forward speed from accelerometer jiggle in aquatic environments. *J. Exp. Biol.* **221**, jeb170449. doi:10.1242/jeb.170449

Costa, D. P. and Williams, T. M. (1999). Marine mammal energetics. In *Encyclopedia of Marine Mammals* (ed. W. F. Perrin, B. Würsig and J. G. M. Thewissen), pp. 383-391. Academic Press.

Dakin, R., Segre, P. S., Straw, A. D. and Altshuler, D. L. (2018). Morphology, muscle capacity, skill, and maneuvering ability in hummingbirds. *Science* **359**, 653-657. doi:10.1126/science.aao7104

Denny, M. (1988). *Biology and the Mechanics of the Wave-Swept Environment*. Princeton University Press.

Dewar, H. and Graham, J. B. (1994). Studies of tropical tuna swimming performance in a large water tunnel. *J. Exp. Biol.* **15**, 13-31.

Donley, J. M., Sepulveda, C. A., Konstantinidis, P., Gemballa, S. and Shadwick, R. E. (2004). Convergent evolution in mechanical design of lamnid sharks and tunas. *Nature* **429**, 61-65. doi:10.1038/nature02435

Durban, J. W., Fearnbach, H., Barrett-Lennard, L. G., Perryman, W. L. and Leroi, D. J. (2015). Photogrammetry of killer whales using a small hexacopter launched at sea. *J. Unmanned Veh. Syst.* **3**, 131-135. doi:10.1139/juvs-2015-0020

Fearnbach, H., Durban, J., Parsons, K. and Claridge, D. (2012). Photographic mark–recapture analysis of local dynamics within an open population of dolphins. *Ecol. Appl.* **22**, 1689-1700. doi:10.1890/12-0021.1

Fish, F. E. (1993). Power output and propulsie efficiency of swimming bottlenose dolphins (Tursiops truncatus). *J. Exp. Biol.* **15**, 179-193.

Fish, F. E. (1996). Transitions from drag-based to lift-based propulsion in mammalian swimming. *Am. Zool.* **36**, 628-641. doi:10.1093/icb/36.6.628

Fish, F. E. (1998). Compartive kinematics and hydrodynamics of odontocete cetaceans: morphological and ecological correlates with swimming performance. *J. Exp. Biol.* **11**, 2867-2877.

Fish, F. E. (2001). A mechanism for evolutionary transition in swimming mode by mammals. In *Secondary Adaptation of Tetrapods to Life in Water* (ed. J.-M. Mazin and V. De Buffrenil), p. 27. Pfeil.

Fish, F. E. and Lauder, G. V. (2006). Passive and active flow control by swimming fishes and mammals. *Annu. Rev. Fluid Mech.* **38**, 193-224. doi:10.1146/annurev.fluid.38.050304.092201

Fish, F. E. and Lauder, G. V. (2017). Control surfaces of aquatic vertebrates: active and passive design and function. *J. Exp. Biol.* **220**, 4351-4363. doi:10.1242/jeb.149617

Fish, F. E. and Rohr, J. J. (1999). *Review of Dolphin Hydrodynamics and Swimming Performance*. Fort Belvoir, VA: Defense Technical Information Center.

Fish, F. E. and Shannahan, L. D. (2000). The role of the pectoral fins in body trim of sharks. *J. Fish Biol.* **56**, 1062-1073. doi:10.1111/j.1095-8649.2000.tb02123.x

Fish, F. E., Hurley, J. and Costa, D. P. (2003). Maneuverability by the sea lion Zalophus californianus: turning performance of an unstable body design. *J. Exp. Biol.* **206**, 667-674. doi:10.1242/jeb.00144

Fish, F. E., Nicastro, A. J. and Weihs, D. (2006). Dynamics of the aerial maneuvers of spinner dolphins. *J. Exp. Biol.* **209**, 590-598. doi:10.1242/jeb.02034

Fish, F. E., Legac, P., Williams, T. M. and Wei, T. (2014). Measurement of hydrodynamic force generation by swimming dolphins using bubble DPIV. *J. Exp. Biol.* **217**, 252-260. doi:10.1242/jeb.087924

Fish, F., Williams, T., Sherman, E., Moon, Y., Wu, V. and Wei, T. (2018). Experimental measurement of dolphin thrust generated during a tail stand using DPIV. *Fluids* **3**, 33. doi:10.3390/fluids3020033

Full, R. J., Kubow, T., Schmitt, J., Holmes, P. and Koditschek, D. (2002). Quantifying dynamic stability and maneuverability in legged locomotion. *Integr. Comp. Biol.* **42**, 149-157. doi:10.1093/icb/42.1.149

Gazzola, M., Argentina, M. and Mahadevan, L. (2014). Scaling macroscopic aquatic locomotion. *Nat. Phys.* **10**, 758-761. doi:10.1038/nphys3078

Gleiss, A. C., Jorgensen, S. J., Liebsch, N., Sala, J. E., Norman, B., Hays, G. C., Quintana, F., Grundy, E., Campagna, C., Trites, A. W. et al. (2011). Convergent

evolution in locomotory patterns of flying and swimming animals. *Nat. Commun.* **2**, 352. doi:10.1038/ncomms1350
Gleiss, A. C., Potvin, J. and Goldbogen, J. A. (2017). Physical trade-offs shape the evolution of buoyancy control in sharks. *Proc. R. Soc. B Biol. Sci.* **284**, 20171345. doi:10.1098/rspb.2017.1345
Goldbogen, J. A. and Madsen, P. T. (2018). The evolution of foraging capacity and gigantism in cetaceans. *J. Exp. Biol.* **221**, jeb166033. doi:10.1242/jeb.166033
Goldbogen, J. A., Calambokidis, J., Shadwick, R. E., Oleson, E. M., McDonald, M. A. and Hildebrand, J. A. (2006). Kinematics of foraging dives and lunge-feeding in fin whales. *J. Exp. Biol.* **209**, 1231-1244. doi:10.1242/jeb.02135
Goldbogen, J. A., Calambokidis, J., Oleson, E., Potvin, J., Pyenson, N. D., Schorr, G. and Shadwick, R. E. (2011). Mechanics, hydrodynamics and energetics of blue whale lunge feeding: efficiency dependence on krill density. *J. Exp. Biol.* **214**, 698-699. doi:10.1242/jeb.054726
Goldbogen, J. A., Calambokidis, J., Friedlaender, A. S., Francis, J., DeRuiter, S. L., Stimpert, A. K., Falcone, E. and Southall, B. L. (2012). Underwater acrobatics by the world's largest predator: 360° rolling manoeuvres by lunge-feeding blue whales. *Biol. Lett.* **9**, 20120986. doi:10.1098/rsbl.2012.0986
Goldbogen, J. A., Cade, D. E., Calambokidis, J., Friedlaender, A. S., Potvin, J., Segre, P. S. and Werth, A. J. (2017). How Baleen whales feed: the biomechanics of engulfment and filtration. *Annu. Rev. Mar. Sci.* **9**, 367-386. doi:10.1146/annurev-marine-122414-033905
Graham, J. B., Dewar, H., Lai, N. C., Lowell, W. R. and Arce, S. M. (1990). Aspects of shark swimming performance determined using a large water tunnel. *J. Exp. Biol.* **18**, 175-192.
Hamilton, J. L., Dillaman, R. M., McLellan, W. A. and Pabst, D. A. (2004). Structural fiber reinforcement of keel blubber in harbor porpoise (Phocoena phocoena). *J. Morphol.* **261**, 105-117. doi:10.1002/jmor.10232
Han, A. X., Berlin, C. and Ellerby, D. J. (2017). Field swimming behavior in largemouth bass deviates from predictions based on economy and propulsive efficiency. *J. Exp. Biol.* **220**, 3204-3208. doi:10.1242/jeb.158345
Hein, A. M., Hou, C. and Gillooly, J. F. (2012). Energetic and biomechanical constraints on animal migration distance. *Ecol. Lett.* **15**, 104-110. doi:10.1111/j.1461-0248.2011.01714.x
Higham, T. E., Rogers, S. M., Langerhans, R. B., Jamniczky, H. A., Lauder, G. V., Stewart, W. J., Martin, C. H. and Reznick, D. N. (2016). Speciation through the lens of biomechanics: locomotion, prey capture and reproductive isolation. *Proc. R. Soc. B Biol. Sci.* **283**, 20161294. doi:10.1098/rspb.2016.1294
Hill, A. V. (1950). The dimensions of animals and their muscular dynamics. *Sci. Prog.* **23**, 209-230.
Johnson, M. P. and Tyack, P. L. (2003). A digital acoustic recording tag for measuring the response of wild marine mammals to sound. *IEEE J. Ocean. Eng.* **28**, 3-12. doi:10.1109/JOE.2002.808212
Kermack, K. A. (1948). The propulsive powers of blue and fin whales. *J. Exp. Biol.* **4**, 237-240.
Kleiber, M. (1975). Metabolic turnover rate: a physiological meaning of the metabolic rate per unit body weight. *J. Theor. Biol.* **53**, 199-204. doi:10.1016/0022-5193(75)90110-1
Kohannim, S. and Iwasaki, T. (2014). Analytical insights into optimality and resonance in fish swimming. *J. R. Soc. Interface* **11**, 20131073. doi:10.1098/rsif.2013.1073
Kooyman, G. L. (1989). *Diverse Divers: Physiology and Behavior*. Springer Science & Business Media.
Kreyszig, E. (2016). *Advanced Engineering Mathematics*, 10th edn. John Wiley & Sons.
Lighthill, M. J. (1970). Aquatic animal propulsion of high hydromechanical efficiency. *J. Fluid Mech.* **44**, 265. doi:10.1017/S0022112070001830
Lockyer, C. (1981). Growth and energy budgets of large baleen whales from the Southern Hemisphere. XF2006134403 FAO Fisheries Series 5, 379-487.
Long, J. H., Koob-Emunds, M., Sinwell, B. and Koob, T. J. (2002). The notochord of hagfish Myxine glutinosa: visco-elastic properties and mechanical functions during steady swimming. *J. Exp. Biol.* **205**, 3819-3831.
Martin López, L. M., Miller, P. J. O., Aguilar de Soto, N. and Johnson, M. (2015). Gait switches in deep-diving beaked whales: biomechanical strategies for long-duration dives. *J. Exp. Biol.* **218**, 1325-1338. doi:10.1242/jeb.106013
Martín López, L. M., Aguilar de Soto, N., Miller, P. and Johnson, M. (2016). Tracking the kinematics of caudal-oscillatory swimming: a comparison of two on-animal sensing methods. *J. Exp. Biol.* **219**, 2103-2109. doi:10.1242/jeb.136242
McClain, C. R., Balk, M. A., Benfield, M. C., Branch, T. A., Chen, C., Cosgrove, J., Dove, A. D. M., Gaskins, L. C., Helm, R. R., Hochberg, F. G. et al. (2015). Sizing ocean giants: patterns of intraspecific size variation in marine megafauna. *PeerJ* **3**, e715. doi:10.7717/peerj.715
Meyer-Vernet, N. and Rospars, J.-P. (2016). Maximum relative speeds of living organisms: why do bacteria perform as fast as ostriches? *Phys. Biol.* **13**, 066006. doi:10.1088/1478-3975/13/6/066006
Motani, R. (2002). Scaling effects in caudal fin propulsion and the speed of ichthyosaurs. *Nature* **415**, 309-312. doi:10.1038/415309a
Pabst, D. A. (1996). Springs in swimming animals. *Am. Zool.* **36**, 723-735. doi:10.1093/icb/36.6.723
Pabst, D. A. (2000). To bend a dolphin: convergence of force transmission designs in cetaceans and scombrid fishes. *Am. Zool.* **40**, 146-155. doi:10.1093/icb/40.1.146
Parry, D. A. (1949). The swimming of whales and a discussion of Gray's paradox. *J. Exp. Biol.* **26**, 24-28.
Pennycuick, C. J. (1975). Mechanics of flight. *Avian Biol.* **V**, 1-75. doi:10.1016/B978-0-12-249405-5.50009-4
Pennycuick, C. J. (1992). *Newton Rules Biology*. Oxford University Press.
Putch, A. (2017). Linear measurement accuracy of DJI drone platforms and photogrammetry. San Francisco: DroneDeploy.
Pyenson, N. D. (2017). The ecological rise of whales chronicled by the fossil record. *Curr. Biol.* **27**, R558-R564. doi:10.1016/j.cub.2017.05.001
Rohr, J. J. and Fish, F. E. (2004). Strouhal numbers and optimization of swimming by odontocete cetaceans. *J. Exp. Biol.* **207**, 1633-1642. doi:10.1242/jeb.00948
Sato, K., Watanuki, Y., Takahashi, A., Miller, P. J. O., Tanaka, H., Kawabe, R., Ponganis, P. J., Handrich, Y., Akamatsu, T., Watanabe, Y. et al. (2007). Stroke frequency, but not swimming speed, is related to body size in free-ranging seabirds, pinnipeds and cetaceans. *Proc. R. Soc. B Biol. Sci.* **274**, 471-477. doi:10.1098/rspb.2006.0005
Schindelin, J., Arganda-Carreras, I., Frise, E., Kaynig, V., Longair, M., Pietzsch, T., Preibisch, S., Rueden, C., Saalfeld, S., Schmid, B. et al. (2012). Fiji: an open-source platform for biological-image analysis. *Nat. Methods* **9**, 676-682. doi:10.1038/nmeth.2019
Schmidt-Nielsen, K. (1972). Locomotion: energy cost of swimming, flying, and running. *Sci. New Ser.* **177**, 222-228. doi:10.1126/science.177.4045.222
Scholander, P. F. (1940). *Experimental Investigations on the Respiratory Function in Diving Mammals and Birds*. Oslo: I kommisjon hos Jacob Dybwad.
Segre, P. S., Cade, D. E., Fish, F. E., Potvin, J., Allen, A. N., Calambokidis, J., Friedlaender, A. S. and Goldbogen, J. A. (2016). Hydrodynamic properties of fin whale flippers predict maximum rolling performance. *J. Exp. Biol.* **219**, 3315-3320. doi:10.1242/jeb.137091
Segre, P. S., Cade, D. E., Calambokidis, J., Fish, F. E., Friedlaender, A. S., Potvin, J. and Goldbogen, J. A. (2018). body flexibility enhances maneuverability in the world's largest predator. *Integr. Comp. Biol.* **59**, 48-60. doi:10.1093/icb/icy121
Shadwick, R. E. and Gemballa, S. (2005). Structure, kinematics, and muscle dynamics in undulatory swimming. *Fish Physiol.* **23**, 241-280. doi:10.1016/S1546-5098(05)23007-8
Simon, M., Johnson, M. and Madsen, P. T. (2012). Keeping momentum with a mouthful of water: behavior and kinematics of humpback whale lunge feeding. *J. Exp. Biol.* **215**, 3786-3798. doi:10.1242/jeb.071092
Slater, G. J., Goldbogen, J. A. and Pyenson, N. D. (2017). Independent evolution of baleen whale gigantism linked to Plio-Pleistocene ocean dynamics. *Proc. R. Soc. B Biol. Sci.* **284**, 20170546. doi:10.1098/rspb.2017.0546
Sumich, J. L. (1983). Swimming velocities, breathing patterns, and estimated costs of locomotion in migrating gray whales, *Eschrichtius robustus*. *Can. J. Zool.* **61**, 647-652. doi:10.1139/z83-086
Taylor, G. K., Nudds, R. L. and Thomas, A. L. R. (2003). Flying and swimming animals cruise at a Strouhal number tuned for high power efficiency. *Nature* **425**, 707-711. doi:10.1038/nature02000
Triantafyllou, M. S., Triantafyllou, G. S. and Gopalkrishnan, R. (1991). Wake mechanics for thrust generation in oscillating foils. *Phys. Fluids Fluid Dyn.* **3**, 2835-2837. doi:10.1063/1.858173
van der Hoop, J. M., Nowacek, D. P., Moore, M. J. and Triantafyllou, M. S. (2017). Swimming kinematics and efficiency of entangled North Atlantic right whales. *Endanger. Species Res.* **32**, 1-17. doi:10.3354/esr00781
Vogel, S. (2008). Modes and scaling in aquatic locomotion. *Integr. Comp. Biol.* **48**, 702-712. doi:10.1093/icb/icn014
Wardle, C. S. (1975). Limit of fish swimming speed. *Nature* **255**, 725-727. doi:10.1038/255725a0
Watanabe, Y. Y., Sato, K., Watanuki, Y., Takahashi, A., Mitani, Y., Amano, M., Aoki, K., Narazaki, T., Iwata, T., Minamikawa, S. et al. (2011). Scaling of swim speed in breath-hold divers: scaling of swim speed. *J. Anim. Ecol.* **80**, 57-68. doi:10.1111/j.1365-2656.2010.01760.x
Watanabe, Y. Y., Goldman, K. J., Caselle, J. E., Chapman, D. D. and Papastamatiou, Y. P. (2015). Comparative analyses of animal-tracking data reveal ecological significance of endothermy in fishes. *Proc. Natl. Acad. Sci. USA* **112**, 6104-6109. doi:10.1073/pnas.1500316112
Watanabe, Y. Y., Payne, N. L., Semmens, J. M., Fox, A. and Huveneers, C. (2019). Swimming strategies and energetics of endothermic white sharks during foraging. *J. Exp. Biol.* **222**, jeb185603. doi:10.1242/jeb.185603
Webb, P. W. (1975). Hydrodynamics and energetics of fish propulsion. *Bull. Fish. Res. Board Can.* **190**, 1-159.
Webb, P. W. (1997). Designs for stability and maneuverability in aquatic vertebrates: What can we learn? In *Proceedings of the Tenth International Symposium on Unmanned Untethered Submersible Technology: Proceedings of the special session on bio-engineering research related to autonomous underwater vehicles*, pp. 86-103. Lee, NH: Autonomous Undersea Systems Institute.

Webb, P. W. and De Buffrénil, V. (1990). Locomotion in the biology of large aquatic vertebrates. *Trans. Am. Fish. Soc.* **119**, 629-641. doi:10.1577/1548-8659(1990)119<0629:LITBOL>2.3.CO;2

Weihs, D. (1973). Optimal fish cruising speed. *Nature* **245**, 48-50. doi:10.1038/245048a0

Williams, T. M. (1999). The evolution of cost efficient swimming in marine mammals: limits to energetic optimization. *Philos. Trans. R. Soc. Lond. B. Biol. Sci.* **354**, 193-201. doi:10.1098/rstb.1999.0371

Williams, R. and Noren, D. P. (2009). Swimming speed, respiration rate, and estimated cost of transport in adult killer whales. *Mar. Mammal Sci.* **25**, 327-350. doi:10.1111/j.1748-7692.2008.00255.x

Williams, T. M., Friedl, W. A. and Haun, J. E. (1993). The physiology of bottlenose dolphins (Tursiops truncatus): heart rate, metabolic rate and plasma lactate concentration during exercise. *J. Exp. Biol.* **179**, 31-46.

Williams, T. M., Wolfe, L., Davis, T., Kendall, T., Richter, B., Wang, Y., Bryce, C., Elkaim, G. H. and Wilmers, C. C. (2014). Instantaneous energetics of puma kills reveal advantage of felid sneak attacks. *Science* **346**, 81-85. doi:10.1126/science.1254885

Woodward, B. L., Winn, J. P. and Fish, F. E. (2006). Morphological specializations of baleen whales associated with hydrodynamic performance and ecological niche. *J. Morphol.* **267**, 1284-1294. doi:10.1002/jmor.10474

Table S1. Tag Deployment Information

Click here to Download Table S1